

## Article

# Experimental Characterization of Memory Effect, Anomalous Self-Preservation and Ice-Hydrate Competition, during Methane-Hydrates Formation and Dissociation in a Lab-Scale Apparatus

Alberto Maria Gambelli \*  and Federico Rossi 

Engineering Department, University of Perugia, Via G. Duranti 93, 06125 Perugia, Italy; federico.rossi@unipg.it

\* Correspondence: albertomaria.gambelli@unipg.it



**Citation:** Gambelli, A.M.; Rossi, F. Experimental Characterization of Memory Effect, Anomalous Self-Preservation and Ice-Hydrate Competition, during Methane-Hydrates Formation and Dissociation in a Lab-Scale Apparatus. *Sustainability* **2022**, *14*, 4807. <https://doi.org/10.3390/su14084807>

Academic Editors: Andrew Adewale Alola, Luigi Aldieri and Uju Violet Alola

Received: 1 March 2022

Accepted: 15 April 2022

Published: 17 April 2022

**Publisher's Note:** MDPI stays neutral with regard to jurisdictional claims in published maps and institutional affiliations.



**Copyright:** © 2022 by the authors. Licensee MDPI, Basel, Switzerland. This article is an open access article distributed under the terms and conditions of the Creative Commons Attribution (CC BY) license (<https://creativecommons.org/licenses/by/4.0/>).

**Abstract:** This study explores the process of methane hydrate formation and dissociation in a small-scale confined environment and in the presence of a porous sediment. The research is focused on answering the shortage of information about the intrinsic properties of the hydrate formation and dissociation processes, such as memory effect and anomalous self-preservation, in a lab-scale apparatus. Experiments were carried out consecutively and with the same gas–water mixture. The temperature reached during dissociation was high enough to ensure the complete dissolution of water cages. At the same time, it was sufficiently low to keep the system able to retain the memory of the previous formation of hydrates. Different well-known phenomena were observed and described; memory effect, anomalous self-preservation and competition between ice and hydrates were shown in detail. Experiments confirmed that the memory effect improves the process mainly during the initial nucleation phase, while it does not provide significant changes in the following massive growth phase. Finally, experiments proved that the formation process can be divided in two different steps: the initial intense growth, due to the small difference in local equilibrium conditions, and the subsequent asymptotic growth, which continues until the process is completed.

**Keywords:** methane hydrates; memory effect; anomalous self-preservation; ice–hydrate competition

## 1. Introduction

The formation of gas hydrates requires the simultaneous presence of relatively low temperatures and high pressures. A wide range of thermodynamic conditions are suitable for hydrate formation, mainly as a function of the guest compound involved in the process [1]. The configuration assumed by water molecules produces a permanent electric dipole; the attraction between the positive/negative poles of these molecules generates the water hydrogen bond [2]. In hydrate structures, guest molecules are physically, but not chemically, trapped into water cages. The chemical interaction between hosts and guests only consists of van der Waals forces; the energy required to dissociate a hydrogen bond is about 5 kcal/mol, while the energy for van der Waals bond is equal to 0.3 kcal/mol [2]. For that reason, the interaction between these two compounds is considered exclusively physical [3]. Hydrate structures are composed by five polyhedra and the nomenclature adopted to indicate them is  $n_i^{m_i}$ , where “ $n_i$ ” is the number of edges in the generic face “ $i$ ” and “ $m_i$ ” represents the number of faces having “ $n_i$ ” edges [4]. According to the theorem of Euler, the sum of the faces and vertices is equal to the number of edges plus two. Seven different types of structure have been found to exist [1]; however, only three of them naturally occur in nature: the cubic structure I (sI) [5], the cubic structure II (sII) [6] and the hexagonal structure H (sH) [7]. The first structure, or sI, contains two small pentagonal dodecahedrons ( $5^{12}$ ) and six tetrakaidecahedrons (14-hedra,  $5^{12}6^2$ ). It is able to host guest molecules having diameters ranging from 4.2 to 6 Å [5]. Typical examples of guest compounds for these

structures are methane and carbon dioxide. Methane is able to occupy both types of cavities, dodecahedrons and tetrakaidecahedrons; conversely, carbon dioxide can enter only in the largest cavities. For that reason, the maximum efficiency that can be reached in replacement processes carried out with pure carbon dioxide is approximately equal to 64% [8,9]. The second type of structure, or sII, contains sixteen small pentagonal cavities ( $5^{12}$ ) and eight tetrakaidecahedrons (16-hedra,  $5^{12}6^4$ ) [6]. It may host molecules having smaller diameters than those contained in sI, such as hydrogen, and also slightly higher diameters, in the range of about 6–7 Å, such as propane. The hexagonal structure H has three  $5^{12}$  cages, one  $5^1, 2^6 4^4$  cage and two irregular dodecahedrons ( $4^3 5^6 6^3$ ) [7]. This latter typology is able to encage large-diameter molecules (as large as 9 Å), such as pentane. As well as diameter, the shape of guest molecules also plays a significant role in the formation of hydrates. In particular, the shape of guests is negligible for structures sI and sII, while it becomes crucial for structure H [2].

As the water content of hydrates is approximately equal to 85% or higher the mechanical properties of gas hydrates are close to those of ice [1]. However, Durham and coworkers proved that the strength of methane hydrates can be up to twenty times higher than that of ice [10]. The formation process consists of two different phases: nucleation and massive growth. During nucleation, the first clusters of hydrates form and aggregate with adjacent nuclei, until they reach the so-called “critical size”. Then, the massive growth phase takes place. The nucleation of hydrates is a microscopic process which involves a few hundred molecules (per site of nucleation). Nucleation is not considered a deterministically certain process. Two different typologies of nucleation are possible: homogeneous (HON) and heterogeneous (HEN). The first typology is mainly theoretical and rarely occurs during real processes; hydrate clusters form in the bulk metastable liquid and can dissociate or continue their growth, as a function of density and composition fluctuations. This process depends on an excess of Gibbs free energy between particles of the solute and the solute in solution. The presence of impurities (i.e., dust microparticles, properties of gas–liquid interfaces, etc.) drives the process to heterogeneous nucleation. It often requires lower supercooling than HON, because the growth of a two-dimensional hydrate structure is more probable and needs less energy than a three-dimensional crystal. The time elapsed until the formation of a detectable amount of structures is named “induction time” [11,12]. It represents the time required to move the local conditions from the phase equilibrium boundary to a configuration suitable for fast and massive hydrate formation. It can also be defined as the time needed to go through the metastable region [13]. According to Wang and colleagues [12], the induction time finishes as soon as the first nuclei of hydrates are sufficiently developed to be visible.

Different theories have been defined to describe the hydrate-formation process. The first of them belongs to Sloan and Fleyfel [14] which, in 1991, characterized the formation of hydrates from ice. Immediately after, Muller-Bongartz and colleagues extended the theory to direct formation from liquid water [15]. According to this theory, when thermodynamic conditions are feasible, first hydrate clusters form and diffuse randomly in water. The clusters consist of a guest molecule surrounded by 20–24 water molecules [2]. This process mainly occurs alongside the gas–liquid interface, or where the contemporary presence of and guests occurs. In addition, the Gibbs free energy of nucleation is lower [16]. These clusters can grow via collision and aggregation with other similar structures, thus forming the first hydrate nuclei. In a similar way, these nuclei can continue their growth and reach the critical size. Precisely, on this concept, the labile cluster theory is based. Initially, water absorbs the guest molecules and produces labile clusters. Subsequently, collision and aggregation leads to the first unstable  $5^{12}$  cages. Similarly to clusters, these cages can dissociate or grow via aggregation. When cages share vertices, small sI units are formed; conversely, when they share faces, small sII cages are formed. The process continues until the critical size is reached. Then, the massive growth phase begins and follows a first-order chemical-kinetic equation for time dependence.

As an alternative, Radhakrishnan and Trout proposed, in 2002, the “local structuring nucleation theory” [17]. According to this theory, first, “prehydrate” structures are formed by locally ordered water-guest clusters. Finally, the “blob hypothesis” combines the labile cluster theory with the local structuring nucleation theory [18].

While hydrates nucleation has been proven to be a statistically probable process, the following massive growth phase always assumes a more deterministic trend.

Usually, the representations of hydrate formation on the time axis leads to the same curve typology, which can be approximately described with the following analytical formula:  $y = 1 - e^{-kt}$ , where “ $t$ ” indicates time and “ $k$ ” is a constant depending on the properties of the process. As soon as the nucleation phase is completed, the growth phase starts with a relatively high intensity, then decelerates gradually until the end of the process. Previous works proved that the hydrate-formation process always assumes this specific trend [19,20], and it can also be found elsewhere in the literature. Li [21] and colleagues studied methane hydrate formation and dissociation in the presence of different typologies of a porous medium and, for each of them, different granulometries were analysed. All configurations tested led to the same type of trend: an initial intense formation, followed by a slower phase. However, the amount of the hydrates formed during this second phase is not necessarily lower than the first phase, as clearly shown in [21]. If chemical inhibitors or promoters are not involved in the process, the formation process leads to similar results in terms of the hydrate formed and the overall trend can be well approximated with the equation shown above. However, minor but visible variations often occur; they are associated to the specific configuration of processes and the main variables that characterize them.

In addition to the initial stochastic nucleation phase, several variables can alter the overall processes, including the so-called “memory effect”. When hydrates are formed twice, consecutively, within the same gas–water mixture, the process becomes faster and requires less time to reach completion. Similar to chemical promoters, hydrate-dissociated solutions are more suitable for the process than fresh gas–water mixtures [22,23]. This phenomenon is associated to the tendency of the system to retain a memory of the previous formation of clathrate structures and appears only when hydrates are melted at moderate temperatures.

Two different theories have been thought to describe the memory effect. The memory effect may depend on the permanence of residual structures randomly diffused in water, such as partial hydrate cages, or it might be associated to the presence of persistent hydrate crystallites. Takeya et al. found that, for carbon-dioxide hydrates, the memory effect remained only at melting temperatures below 298 K [24]. The same tendency has also been observed for other guest compounds [25]. A loss of memory does not exclusively depend on the temperature reached during the melting of the hydrates, it is also a function of time. Duchateau studied hydrate formation using a mixture of methane and propane (98/2%) [26]. He observed a drastic reduction in memory effect when hydrates were melted at superheating temperatures, on average 2–4 °C above equilibrium, for almost two hours. A further relevant variable is associated with the sediment in which hydrates are formed and its main properties, such as chemical composition, size, porosity, permeability, etc.

Several researchers have focused their research on the relation between the hydrate-formation process and sediments, mainly analysing the induction time, the hydrate-formation rate and the hydrate distribution in the sediment [27–30]. Studies on methane hydrate formation in fine sediments revealed the process exhibited two different periods [31]. First, hydrates formed at the interface between the gaseous phase and the sediment; then, they formed in the bulk sediment. The process was faster during the first period, similarly to what was observed in [19–21]. In porous sediment, the most relevant parameter is grain size. The comparison between hydrate formation in sand, having, respectively, 150–250  $\mu\text{m}$  and 250–380  $\mu\text{m}$  grain size, proved that a smaller size tendentially favors the process [31]. However, the relationship to grain size is also a function of the type and chemical composition of the sediment. Studies on hydrate formation in the presence of sand and clay revealed that the induction time increased when silica sand with smaller grain size was

used [28]. The main property affecting gas capture was found to be mass transfer, which is strongly related to the grainsize and the chemical compositions of sediments [29]. Besides the physical and geometrical properties, chemical composition may also play a key role in favoring or hindering hydrate formation. Previous studies revealed that even small percentages of inhibiting materials in silica-based porous media may significantly alter the process [32,33]. Hackikubo and coworkers confirmed that particle size is a crucial parameter during hydrate dissociation [34]; during experiments, they also proved that the hydrate dissociation rate is higher in coarse glass sand than in fine silica sand, because water molecules form a thin layer on grains of fine silica sand. Finally, while hydrate formation is favored in the presence of relatively small-size sand grains, the dissociation process is more effective in the presence of larger grains [35].

The present work aims to describe methane hydrate formation in the presence of fresh water and pure silica sand by progressively reducing the time available for the process. Several tests were carried out consecutively in a small-scale experimental apparatus and with the same gas–water mixture. The thermodynamic conditions were always maintained within the range where the system retains a memory of previous processes. The variation in pressure over time was characterized, together with the amount of gas involved in the hydrate formation. All experiments were carried out with the same conditions, the only difference varied was their duration, which was progressively shortened. In conclusion, experiments were carried out in order to balance the advantageous action related to the memory effect, by granting less time to perform the process. In this way, it is possible to verify how the memory effect operates in the system.

## 2. Materials and Methods

### 2.1. Experimental Apparatus

The experimental apparatus consists of a lab-scale reactor, designed to reproduce gas-hydrate formation in marine sediments. A detailed description of the apparatus employed in this study was presented elsewhere in the literature [36]. Only a brief description of the main characteristics is provided. The reactor is entirely made of 316SS and has an internal cylindrical volume equal to 949 cm<sup>3</sup> (7.3 cm diameter; 22.1 cm height), which makes it substantially greater, in term of size, than the reactors used worldwide to study gas hydrates [37]. Two flanges were used to close its ends and each was equipped with a spiral-metallic gasket, model DN8U PN 10/40 316-FG C8 OR. The reactor was positioned in a tank filled with water and glycol, which was connected to a chiller (model GC-LT) and allowed temperature control. This vessel acted as thermostatic bath for the reactor, even if this term is not completely appropriate, to allow heat exchange between the vessel and the surroundings. A scheme of the experimental apparatus, together with a picture of the reactor, are presented in Figure 1.

The gas injection was at the bottom, as shown in Figure 1. In this way, before entering inside the reactor, the gaseous compound goes through a pipe, having high surface/volume ratio, which is immersed in the thermostatic bath and allows the gas to reach the same temperature as the system before reaching the reactor.

Conversely, the upper flange contained all of the required sensors. It also contained a safety valve (model E10 LS/150, maximum pressure rating of 12 MPa and temperature range from 196 to 450 °C) and a channel for gas ejection. This latter element was divided in two subchannels: one of them was used to quickly evacuate the reactor, while the second was connected to a pressure regulator valve with a septum at the end and was used as a gas sampling port.

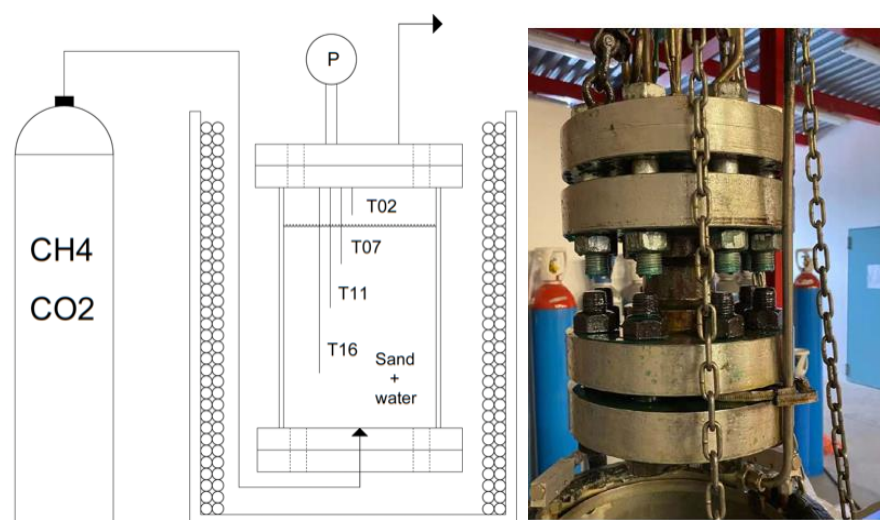


**Figure 1.** Scheme of the experimental apparatus (left) and picture of the lab-scale reactor (right).

Temperature was constantly measured with four Type K thermocouples, having class accuracy 1. These devices were positioned at different depths inside the reactor (respectively, at 2, 7, 11 and 16 cm depth from the upper flange) and allowed the creation of a temperature profile inside the reactor and verification of the possible occurrence of gradients during experiments. The experimental solutions for temperature measurements were selected based on the literature [38–40].

Pressure was measured with a digital manometer, model MAN-SD, having an accuracy equal to  $\pm 0.5\%$  of full scale. Finally, all sensors were connected to a data acquisition system (provided by National Instruments) and managed in LabView.

## 2.2. Materials

Experiments were carried out in the presence of distilled water and pure quartz sand. Initially,  $744 \text{ cm}^3$  of sand was inserted, then followed with  $236 \text{ cm}^3$  of water to fill intergranular space. Sand grains have spherical shape, with diameter approximately equal to  $500 \mu\text{m}$ . Their porosity was measured with a porosimeter (model Thermo Scientific Pascal 140) and was equal to 35%. This value takes into account the free space inside pores and also the free space between grains. Pure methane was employed as the guest compound, consisting of ultra-high-purity (UHP) methane, with purity degree equal to 99.99%.

## 2.3. Experimental Procedure

Initially, the reactor was filled, then the upper flange was closed. Gas injection was performed from the bottom and, during injection, the temperature was kept sufficiently high to avoid hydrate formation. The undesired capture of gaseous molecules into water cages during this phase might cause uncertainties in the accurate definition of quantities involved in the process; thus, it must be avoided. As soon as the target pressure was reached, the injection channel was closed and the reactor started working under batch conditions. During experiments, no mass transfer occurred with the exterior while heat exchange was possible.

Experiments were carried out consecutively and with the same gas–water mixture. Considering the maximum temperatures reached during hydrates dissociation and after the first test, the system benefited from the memory effect. Only temperature was changed externally: it approached the ice point during hydrate formation and was brought to  $14\text{--}15 \text{ }^\circ\text{C}$  during the following dissociation phase. The whole duration of experiments was about 312 h, divided among five tests. While the dissociation of hydrates occurred spontaneously as a consequence of the increased temperature, the formation phase was carried out differently as the time allocated to complete the process was gradually lowered.

Pressure and temperature were directly measured; further parameters were calculated. The ratio between pressure and time was used to describe how the experiment proceeded and, in particular, to verify if the massive growth phase occurred linearly or not and if the memory effect intervened during this phase or if it only acted during the initial nucleation step.

### 3. Results and Discussion

The research was divided into five experiments, where methane hydrate was repeatedly formed and dissociated. Figure 2 shows all the experiments and their pressure and temperature evolution over time.

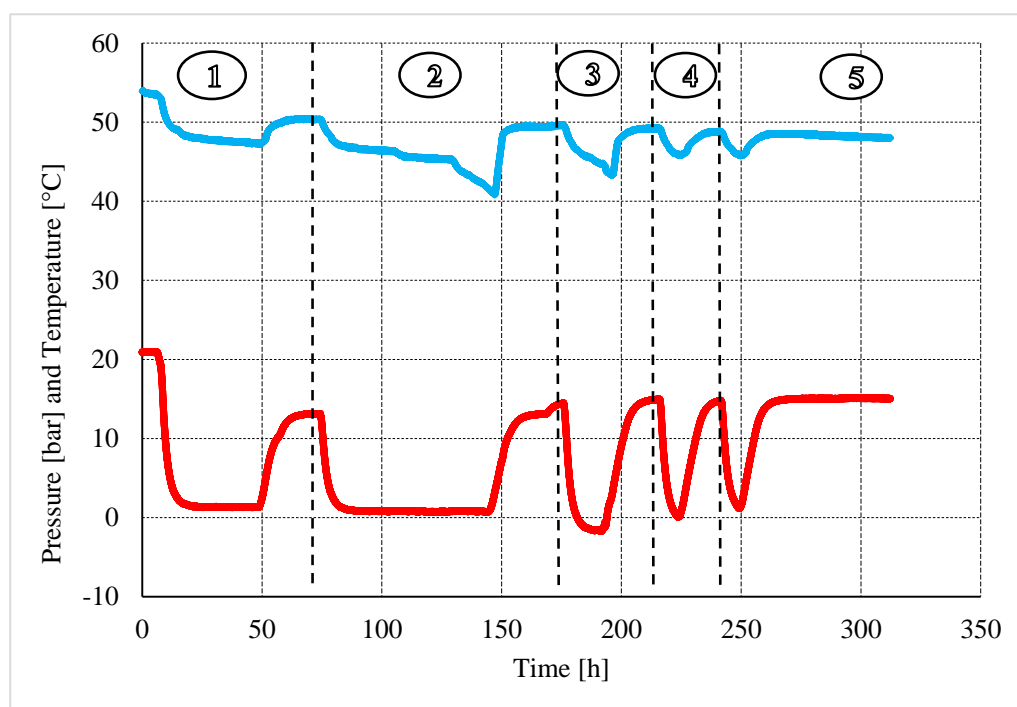


**Figure 2.** Pressure and temperature evolution over time in Tests 1 to 5. Pressure (measured in bar) is shown in blue, while the temperature ( $^{\circ}\text{C}$ ) in red.

Figure 2 clearly shows that the gas injection phase was carried out at temperatures above  $20^{\circ}\text{C}$ , in order to ensure no formation of hydrates during the process. The comparison between the temperature diagram (in red) and the pressure diagram (in blue) reveals a visible decrease in pressure at the beginning of the series, while temperature was still above  $20^{\circ}\text{C}$ . This is mainly due to the diffusion in water of gaseous molecules. Even if the dissolution of methane in water is negligible (equal to  $0.0012 \text{ mol}_{\text{CH}_4}/\text{kg}_{\text{H}_2\text{O}}$ ), considering the relatively little quantity of gas injected inside the reactor, even a small absorption of methane molecules can generate a visible variation in pressure. The diagram has been divided in five regions; each is related to subsequent experiments. Tests were numbered from 1 to 5 and two phases are well distinguishable in all of them: hydrate formation and the subsequent dissociation.

During formation, the temperature was lowered until approaching the ice point (with the exception only of Test 3, where the ice point was reached at slightly lower temperatures). Then, temperature was held constant and the process continued. The formation process finished as soon as the temperature was increased again. While the formation was operator terminated before its completion, the dissociation phase was continued until the solid phase was completely dissolved.

The relation between pressure and temperature is evident, both during formation and dissociation. However, the relationship is not linear and not the same in each test. For

instance, in Test 1 and Test 2, due to the longer availability of time, temperature remained constant and slightly above 0 °C for a certain time period. During this time period, hydrates continued to form, but with a completely different trend when compared with what was observed during the previous temperature drop. Moreover, this phase was not similar between the two experiments. In Test 1, the capture of gas molecules, which is strictly related to the pressure decrease, was slower than what was observed in Test 2, even if the initial conditions were similar. A more detailed description is required for Test 2.

Figure 3 shows the pressure and temperature evolution over time exclusively for Test 2 and provides a better illustration of what was observed during this experiment.

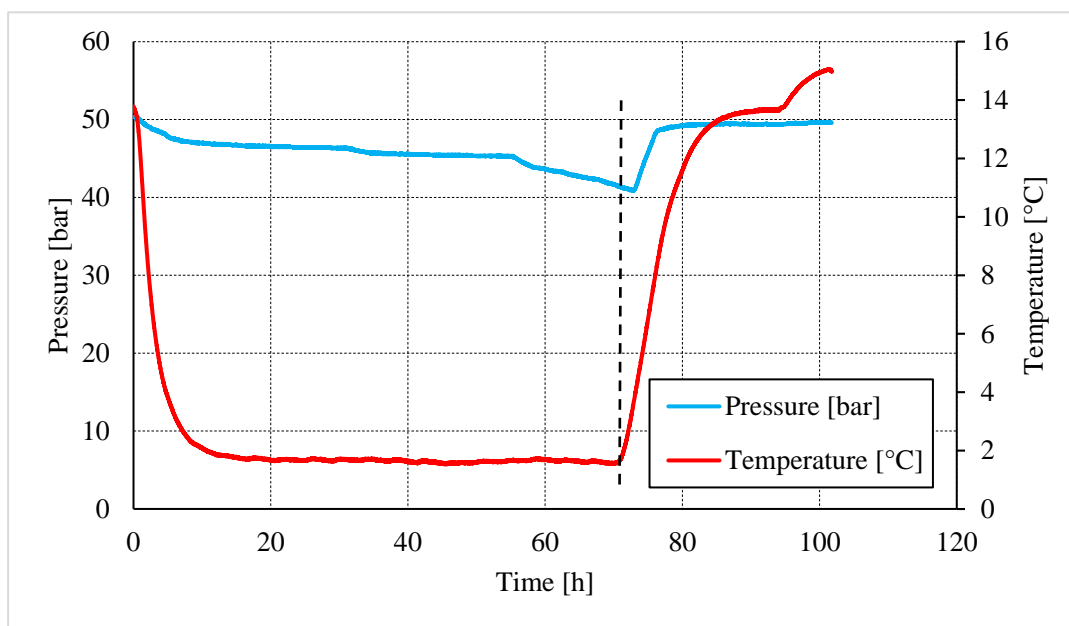


**Figure 3.** Pressure and temperature evolution over time in Test 2.

Figure 3 clearly shows intensive hydrate formation during both the initial temperature drop and during the remaining portion of the formation process, during which temperature remained approximately unchanged. The two trends exhibit only slight differences between each other. Theoretically, the presence of lower temperatures should act as the leading parameter for the process, thus accelerating it; however, the formation rate seemed to be slightly higher during the initial phase, where temperature was still decreasing and the local thermodynamic conditions were closer to the phase-boundary equilibrium. The following drastic reduction in pressure provided a clear explanation of the phenomenon. During the experiments, because of the presence of extremely favorable thermodynamic conditions, the formation process should have proceeded faster. As a consequence of favorable conditions and at the end of the process, the system still had not reached an equilibrium condition. Considering the additional time allowed, the rate of hydrate formation changed significantly. This experiment proved that the relation between these two variables is not linear, nor constant, and cannot be forecast in advance.

Here, as in the following tests, the formation process was interrupted in advance, before its natural conclusion, then an increase in externally imposed temperature caused the gradual dissociation of water cages and the consequent release of methane molecules. During dissociation, pressure often varied with less delay than temperature. This is clearly visible in Figure 3, where vertical lines were used to better show the small delay. As soon as temperature began increasing, pressure continued to decrease, and, after four minutes, the pressure started increasing. This phenomenon is of the so-called “anomalous self-preservation” and consists of the tendency of the system to remain stable for a certain time period, even if outside of the hydrate stability zone [41].

A further decrease in temperature is required for Test 3, where temperature was brought below the ice point during hydrate formation and whose trend over time is shown in Figure 4.

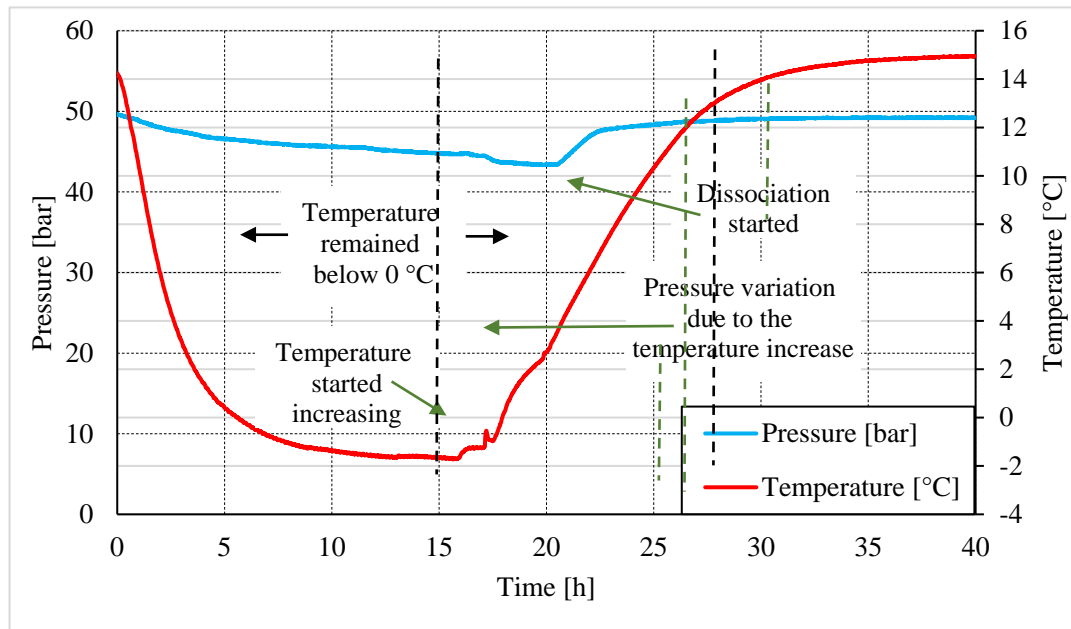


**Figure 4.** Pressure and temperature evolution over time in Test 3.

Figure 4 has two black dotted lines to indicate when temperature moved below  $0\text{ }^{\circ}\text{C}$  and the return above this value. From the left to the right side of the diagram, three green-dotted lines were used to distinguish the three different phases describing the hydrate formation and dissociation processes. The first line indicates when temperature started increasing. The second shows when the increase in temperature caused visible changes in pressure. Finally, the third green line denotes the separation between the formation and dissociation phases. In the first sector, pressure dropped with a higher gradient than the subsequent gradient. When temperature moved below  $0\text{ }^{\circ}\text{C}$ , the pressure decrease was lower than that expected (considering the local thermodynamic condition and their difference with the theoretical phase-boundary equilibrium for methane hydrates). Similar to the previous, Test 2, hydrated dissociation occurred with an evident delay in time, when compared with the temperature diagram. However, such a delay (consisting of the difference in time between the first and the third green line) cannot be explained with the self-preservation of the system. A first reason, shown in Test 2, is that the delay associated to this phenomenon was quantifiable in minutes, while, in Test 3, it was approximately equal to five hours. Secondly, in Test 2, when temperature started to increase, the pressure remained constant and, after several minutes, the pressure also increased. Here, the increase in temperature caused a completely opposite effect: the pressure continued to drop and even accelerated this process, proving the more intense formation of hydrates in this phase. The second green line denotes when the pressure changed its trend: the formation process accelerated significantly, even producing a small visible local peak in temperature associated to the exothermicity of the reaction. The dissociation phase began only after the temperature approached  $4\text{ }^{\circ}\text{C}$ .

In conclusion, in this test, the self-preservation effect did not occur, because the temperature increase was initially responsible for a more intense formation of the hydrate. Differently, the time distance between the first and the second green lines can be associated to the delay, which often occurs, between the establishment of suitable conditions for hydrates and when the process effectively occurs.

This experiment confirmed what has been asserted in the literature about the competition between ice and hydrates [42]. As soon as temperature reached the ice point, ice formation inevitably started inside the reactor, thus reducing the free space and also decreasing the availability of liquid water molecules. This led to a decrease in hydrate formation. The following increase in temperature stopped this process and immediately caused ice melting (the temperatures reached in the previous time periods were only slightly lower than 0 °C). The melting of ice and the presence of a temperature very close to 0 °C made the current thermodynamic conditions the most feasible, of the entire experiment, for hydrate formation and explains the highest rate of gas capture reached in this phase.

As previously described in Section 2, experiments were carried out consecutively and with the same gas–water mixture. Considering the maximum temperatures reached inside the reactor during hydrates dissociation and according to the literature, excepting Test 1, the system retained a memory of the previous formation of hydrates, thus enhancing the process during subsequent tests. This aspect was observed and clearly appears in Figure 1. In Test 1, the pressure drop associated with gas capture into water cages was less pronounced than in other tests, even if it was the only experiment during which the formation phase was not externally terminated and continued until pressure stabilized inside the reactor (thus denoting the completion of the process). Such a difference proved the so-called memory effect occurred and inevitably promoted the process, leading to higher quantities of hydrates.

Table 1 shows, for each test, the time spent during formation, the observed pressure drop and the final pressure value.

**Table 1.** Time spent, pressure drop observed and final pressure reached during hydrate formation in tests 1 to 5.

	$\Delta t$ [h]	$\Delta P_{\text{form}}$ [bar]	$P_f$ [bar]
Test 1	45.3	6.04	47.22
Test 2	72.9	9.5	40.85
Test 3	20.5	6.29	43.36
Test 4	7.75	2.97	45.85
Test 5	8.6	3.42	45.82

The time employed for the formation process constantly decreased; in Test 1, it was slower than in the other experiments, because the pressure stabilized and further time would not have led to any additional information. Finally, the last two tests were carried out for approximately the same time. Parameter  $\Delta P_{\text{form}}$  confirms the contribution of the memory effect: the difference between Test 1 and Test 2 is meaningful. Even without a time restriction, the previous decrease in Test 1 was drastically lower than Test 2. In the later experiment, the relation between time spent and pressure drop remained substantially unchanged. This proves the memory effect did not increase its contribution significantly with the results of the experiments. Time only ensured a strong difference between hydrate formation and its absence. The ratio between the pressure drop observed during formation and the time to cause hydrate formation is shown in Table 2.

**Table 2.** Ratio between pressure drop (which is strictly related to the amount of hydrate formed) and the time spent for the formation process, calculated for each experiment.

	$\Delta P_{\text{form}}/\Delta t$ [bar/h]
Test 1	0.13
Test 2	0.13
Test 3	0.31
Test 4	0.38
Test 5	0.40

Results shown in Table 2 seem to confirm what was previously asserted; however, with two inconsistencies. The ratio of pressure decrease and time assumed the same value in Test 1 and Test 2 and did not reflect what effectively happened in terms of hydrate formation. While that value is acceptable for Test 1, it did not adequately describe Test 2. Moreover, the value measured in Test 3 should have been nearer to that observed in Tests 4 and 5.

This latter inconsistency can be easily explained with the lower hydrate formation observed in this test, due to the formation of ice crystals and the consequent competition between these two compounds. Differently, the similarity between the first two tests needs to be better described. In Tests 3 to 5, the formation of hydrates was interrupted before its completion; thus, the mean variation of pressure over time is higher than in Tests 1 and 2. This concept is quite visible in the subsequent panels of Figure 5, where the evolution of parameter  $\Delta P_{\text{form}}/\Delta t$  over time is shown.

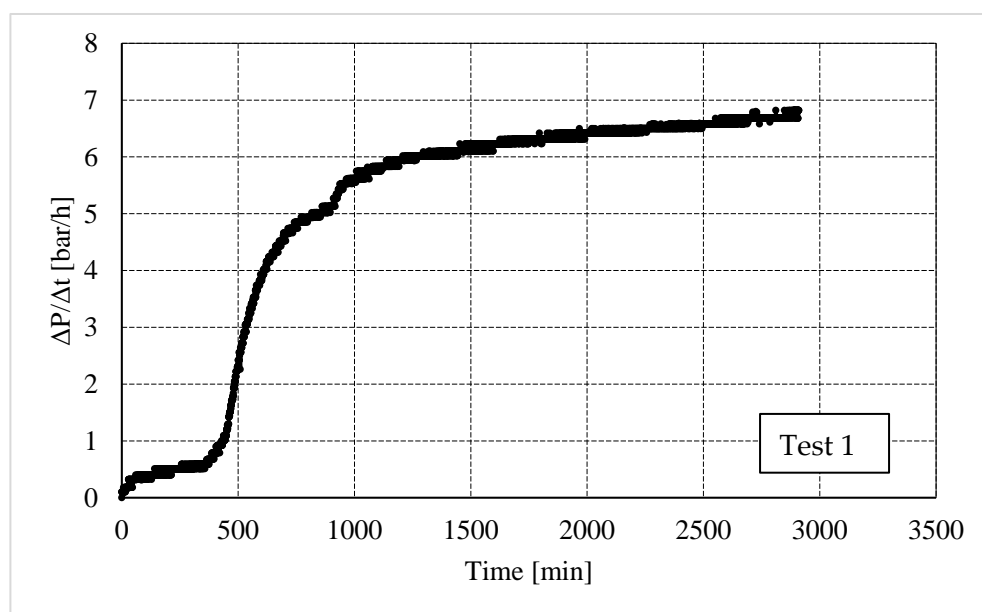


Figure 5. Cont.

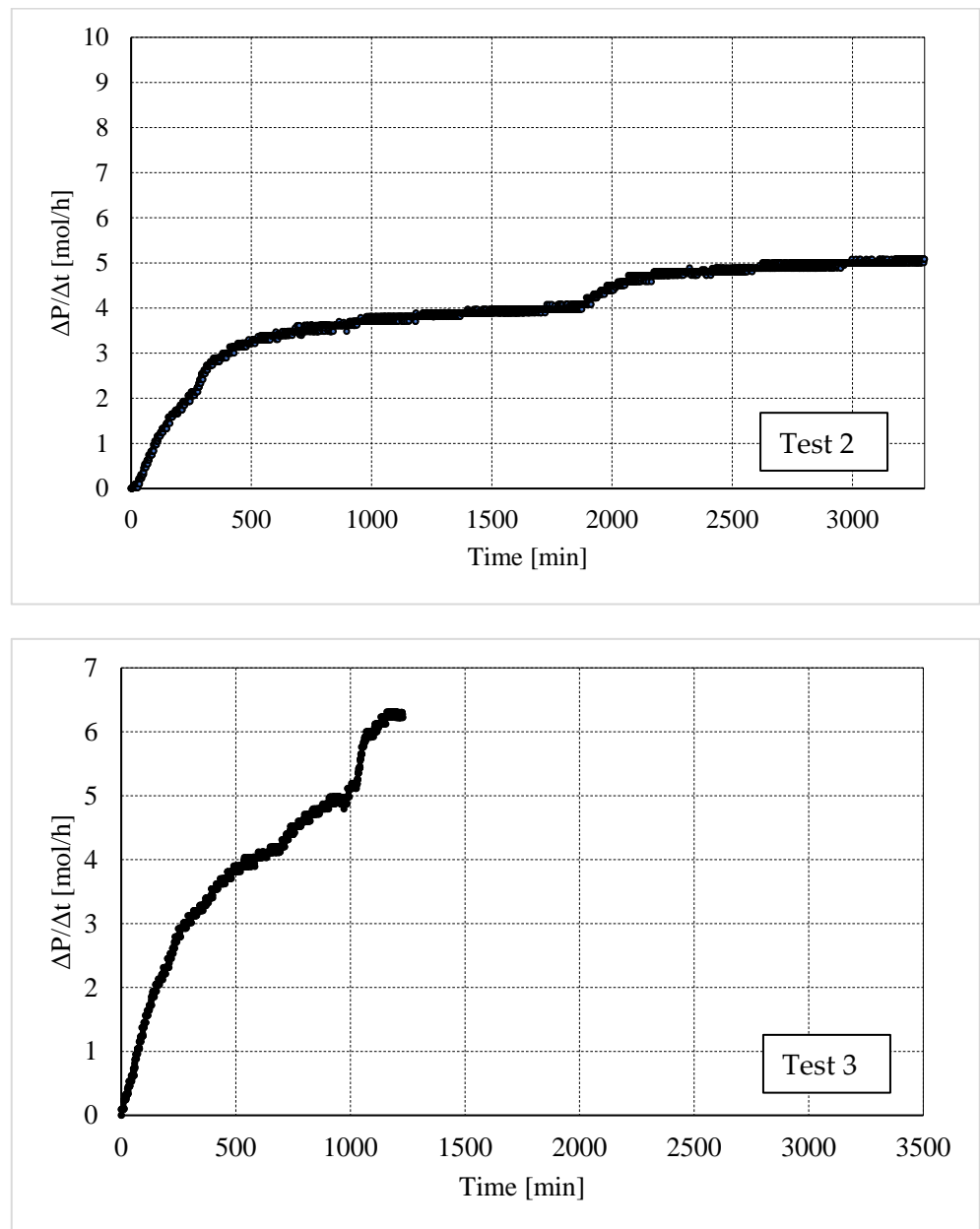
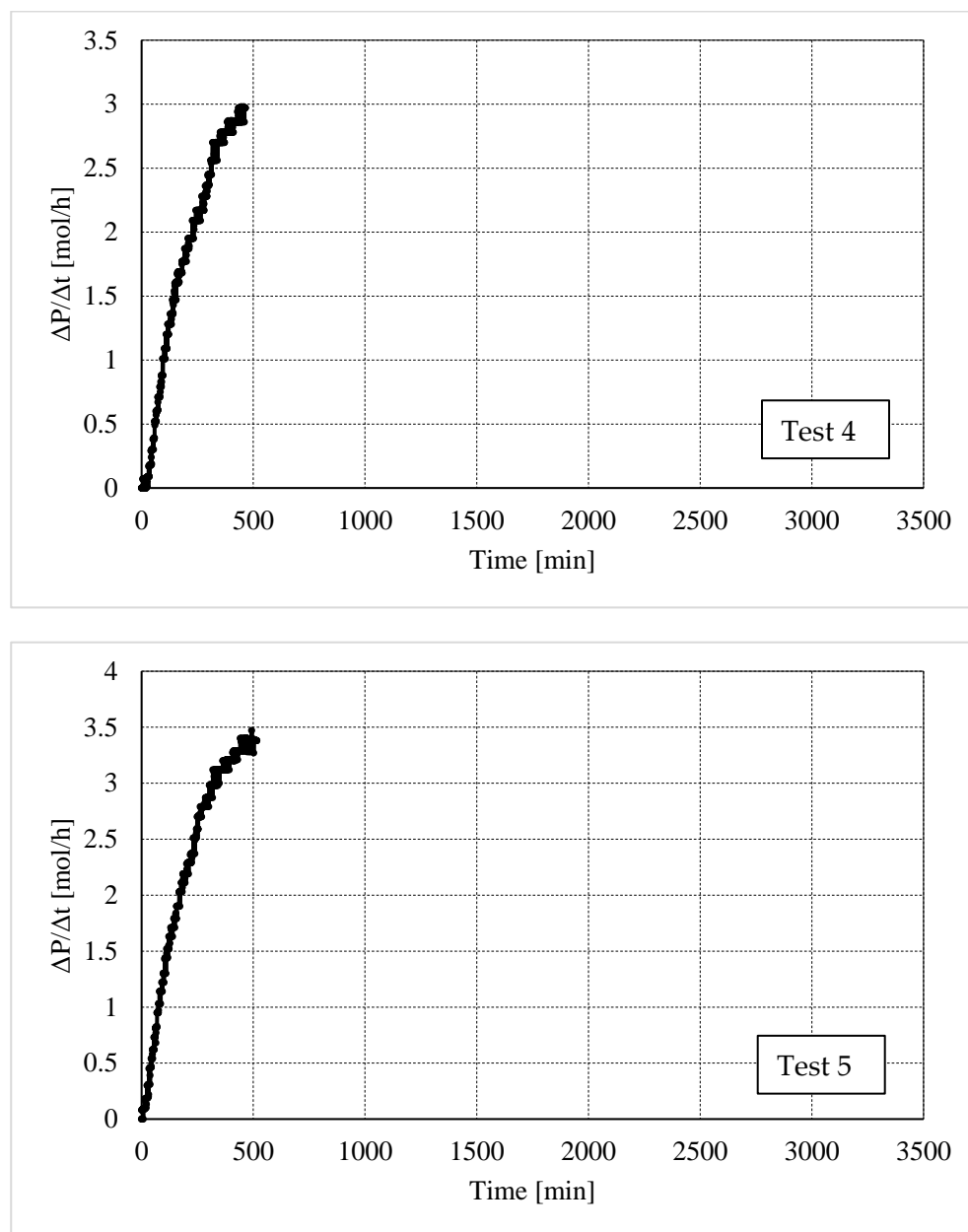


Figure 5. Cont.



**Figure 5.** Evolution of parameter  $\Delta P_{\text{form}}/\Delta t$  during hydrate formation in Tests 1–5.

These diagrams demonstrated clearly how the memory effect controlled the hydrate-formation process. As expected, all experiments showed a similar trend, with Test 1 being the only exception. Tests 2–5 confirmed the theory that memory is an advantage primarily during the nucleation phase. At the beginning of Test 1 (during which the memory effect was clearly absent), the process proceeded slowly, while, in all other experiments, it started rapidly. The trends observed in successive panels of Figure 5 allowed to answer the critical question emerging from the evaluation of Table 2. The values shown in Table 2 do not reveal any difference between Test 1 and Test 2; however, the memory effect should have provided a positive contribution during Test 2 (compared with Test 1). The diagrams proved that the hydrate-formation process in Test 2 was extremely similar to what was observed in Tests 3–5, while it was noticeably different than the trend observed for Test 1. This aspect was numerically demonstrated in Table 3, where the same parameter,  $\Delta P_{\text{form}}/\Delta t$ , shown in Table 2 was calculated again but only for a limited time period, or for the first 500 min of each test. Therefore, in the last three experiments, the formation process was interrupted

before its completion, while, in the first two tests, there was the possibility of reaching equilibrium inside the reactor. The comparison was more coherent when performed in the first portion of the formation process, which occurred in all experiments and not in the whole process.

**Table 3.** Ratio between pressure drop (which is strictly related to the amount of hydrate formed) and the first 500 min spent in the formation process, as calculated for each experiment.

	$\Delta P_{\text{form}}/\Delta t$ [bar/h]
Test 1	0.18
Test 2	0.39
Test 3	0.37
Test 4	0.38
Test 5	0.40

Table 3 highlights the difference between Test 1 and Test 2 and the similarity between tests from 2 to 5. In addition, Test 1 showed an increase in parameter  $\Delta P_{\text{form}}/\Delta t$ , from 0.13 to 0.18 bar/h. Also in this test, the last part of the process occurred with a formation rate significantly slower than that assumed at the beginning of the massive formation of hydrates.

In the first two experiments, where the process had the possibility to reach completion, hydrate formation assumed an asymptotic trend that can be approximated with the equation  $y = 1 - e^{-kt}$ . With time, the process reached completion and equilibrium was achieved in the reactor. As the experiments were batch experiments, the internal conditions gradually approached equilibrium and the process decelerates. While the equation approximately describes the hydrate-formation process, the constant “k” must be determined for specific conditions. Future research will exclusively focus on quantifying “k” for specific conditions. For instance, as the phase-boundary equilibrium curves can be described with a general equation but may change significantly as a function of the specific guest molecule (see equilibrium diagrams shown in [2]). In addition, the trend of hydrate formation may vary depending on the guest compound. In sI structures, methane molecules can occupy both the small and the large cavities, ensuring more complete filling of structures. Conversely, carbon dioxide has higher solubility in water, which makes the hydrate-formation process faster. Besides the guest compound, other key parameters must be included in the definition of “k”; among them, the initial thermodynamic condition (including the distance between the thermodynamic condition and the equilibrium-phase boundary). The presence of sediments and their physical properties (granulometry, size, porosity, composition, etc.), also influence the memory effect.

Figure 6 shows the pressure–temperature trend of each experiment. This figure also shows the phase-boundary equilibrium for methane hydrates, using data from the literature [43–51]. In the figures, black dots were used to represent the phase-boundary equilibrium for methane hydrates, while experiments were shown in red. The evolution during the experimental time is indicated with red arrows.

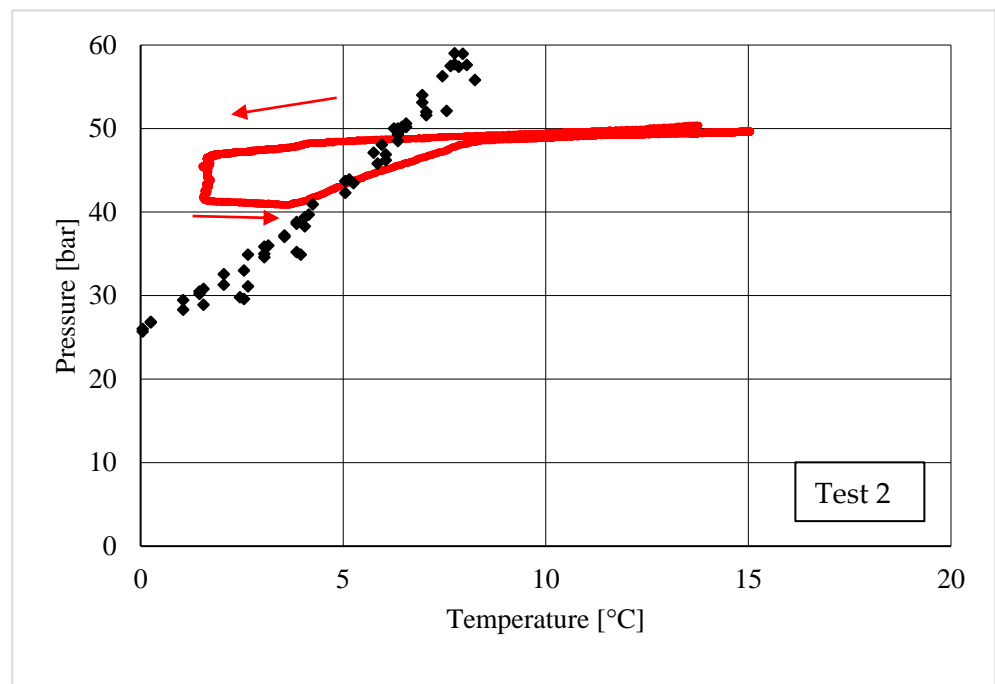
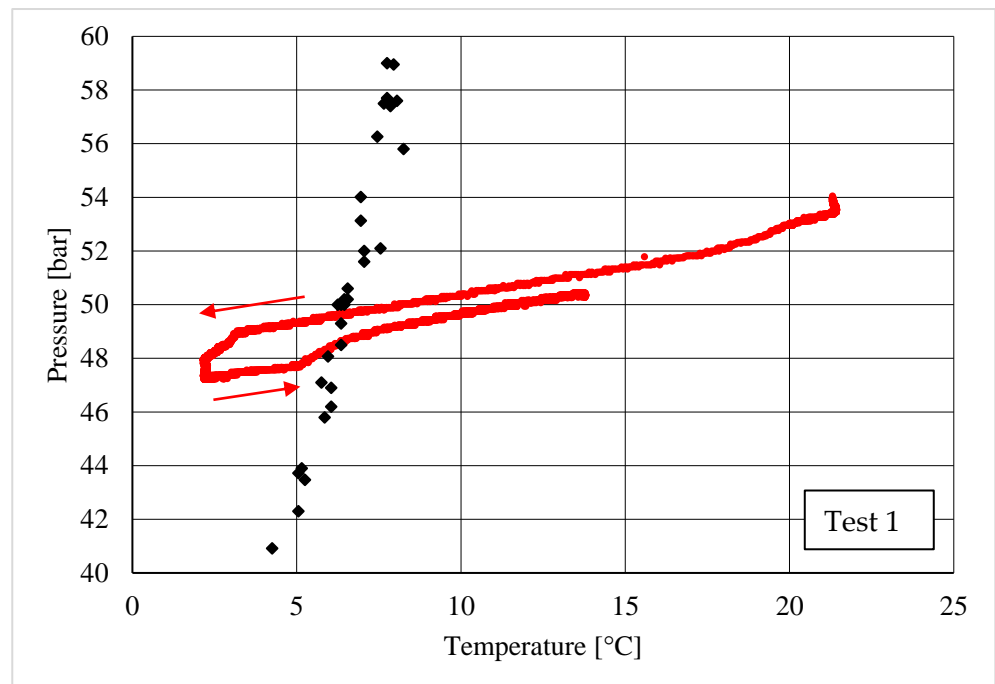


Figure 6. Cont.

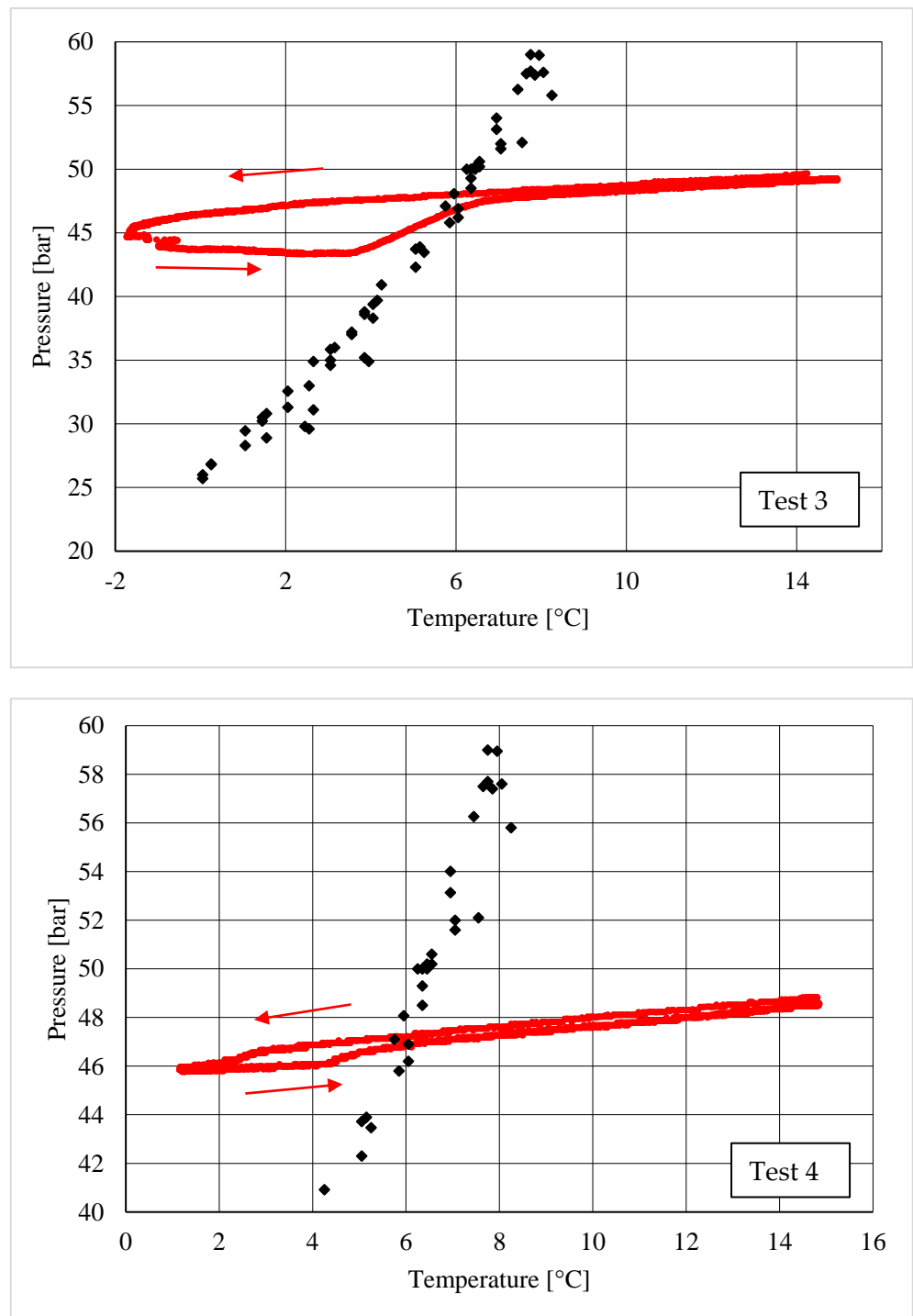
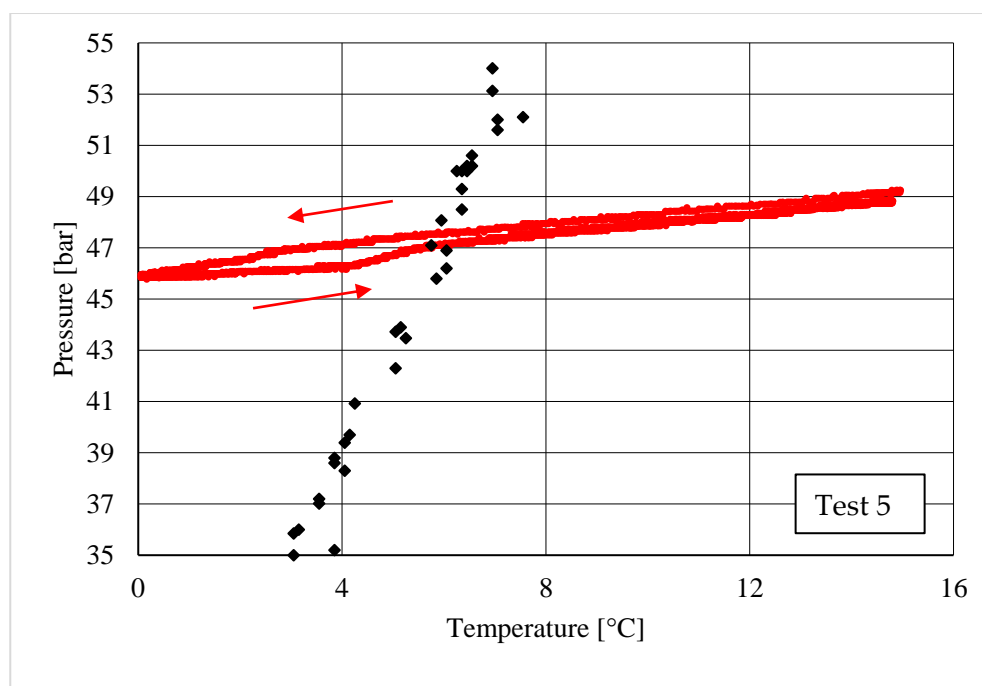


Figure 6. Cont.



**Figure 6.** Description of Tests 1–5 in a pressure–temperature diagram and comparison of tests with the phase-boundary equilibrium (shown with black dots).

The system initially moved from right to left as temperature was decreased and pressure consequently decreased. Conversely, the dissociation phase moved from left to right and shows the increase in pressure to its initial values due to the increase in temperature.

The panels of Figure 6 demonstrated that experiments did not describe the equilibrium conditions for the system: there is no similarity between the experimental and the theoretical values. However, the formation process was verified on the left side of the equilibrium line, or in the methane-hydrates stability zone. On the right side, the pressure varied only as a consequence of the temperature increase/decrease according to the equation of state for gases. For this reason, the formation and dissociation curves almost perfectly overlap, proving the absence of hydrate structures inside the reactor at this step. Only in Test 1 is a visible difference between the two phases apparent. Hydrate-formation and dissociation curves remained parallel as in other tests, but spaced out by about 1.5–2 bar. Test 1 was the first experiment of the series and the dissolution of methane in water occurred during the experiment. Even if the dissolution of methane in water is almost negligible ( $0.0012 \text{ mol}_{\text{CH}_4}/\text{kg}_{\text{H}_2\text{O}}$ ), the relatively low quantity of gas injected inside the reactor and the surplus of water caused an observable decrease in gaseous methane.

As explained above, the formation/dissociation process of hydrates is confirmed in these diagrams, because the relation between pressure and temperature was no longer exclusively dependent on the equation of state and, consequently, the two curves showed meaningful differences between each other. This deviation was verified only at the left of the equilibrium line, where the thermodynamic conditions were suitable for gas hydrate formation.

The only exception to the present discussion was found in Test 2, where the dissociation of hydrates also continued on the right of the equilibrium curve. As explained in the description of Figure 2, the evolution of this experiment was affected by the occurrence of the self-preservation effect, which delayed the process and postponed the dissociation of water structures, which inevitably required higher temperatures.

In these diagrams, the difference between the first two tests and the remaining three was even more evident. Once the minimum temperature was reached during the formation phase in Test 1 and Test 2, the system had enough time to complete the process. The P–T curve has an almost vertical drop, associated to the abundant production of hydrates

at a constant temperature. Then, the dissociation phase began and the system initially moved horizontally to the phase boundary equilibrium, then approached the trend of the latter portion of the curve. The horizontal trend occurred because of the initial stability of hydrates, even if the local temperature was already increasing. It happened because the overall thermodynamic conditions were again suitable for hydrates stability, thus pressure remained unchanged. Finally, the dissociation also started when the internal configuration was close to the theoretical equilibrium values and approached the equilibrium trend. Conversely, the similarity between the experimental dissociation of hydrates and the equilibrium line was completely absent in Tests 3 to 5. That is associated to the modality adopted to carry out experiments. The formation phase was interrupted in advance of the completion of the process of hydrate formation. Consequently, in these tests, the dissociation curve remained close to the formation curve and, consequently, far from the phase-boundary equilibrium.

#### 4. Conclusions

This manuscript analysed methane hydrates formation in a confined environment and in the presence of pure-silica-sand porous medium. Five tests were carried out and the main difference between them consisted of the time spent for hydrate formation. While, in Test 1 and in Test 2, the time was sufficient to reach the process completion, in the other experiments the process was terminated early. The experimental conditions were defined in order to observe and describe with accuracy crucial parameters that play key roles during hydrate formation and dissociation, including the memory effect, anomalous self-preservation and the competition between ice and hydrates. The competition between ice and hydrates was investigated by lowering the internal temperature during the formation phase, until moving slightly below the ice point. Then, temperature was increased again while monitoring pressure variations. The following conclusions were possible:

- (i) The memory effect mainly occurred and led to a substantial difference between the first test and the subsequent test, both in terms of moles of hydrate formed and time required for the process.
- (ii) The memory effect contribution primarily intervened during the initial step of hydrate formation, or during the nucleation phase. Data reported in this work characterized the massive growth phase and proved that it occurred similarly in all experiments.
- (iii) The hydrate-formation and dissociation processes occurred in the hydrate-stability zone; in particular, hydrate dissociation began once the internal thermodynamic conditions approached the phase-boundary equilibrium and then proceeded by showing a certain similarity with the configuration of equilibrium.
- (iv) In some tests, the dissociation of hydrates occurred with a certain delay, when the system had already moved outside of the stability zone. This specific behaviour was associated to the anomalous self-preservation.
- (v) When the temperature was brought below 0 °C, the formation of hydrates decreased significantly and continued when temperature was increased above the ice point. When water molecules have the possibility to organize themselves in a solid crystalline structure without a guest molecule, the formation of hydrates is hindered and cannot be completely associated to the difference between local and equilibrium thermodynamic conditions.

Initially, the relevant distance between the pressure and temperature values and those describing the phase-boundary equilibrium showed the process proceeded intensively and led to the fast formation of hydrates. Then, the system assumed an asymptotic trend until reaching completion. The present description is suitable for each system; however, the formation process can be characterized in advance by defining the influence on the process of primary properties such as the size and shape of the guest compound, the main properties of sediments, the presence or absence of memory, and the initial thermodynamic configuration.

**Author Contributions:** Conceptualization, A.M.G. and F.R.; methodology, A.M.G.; validation, F.R.; formal analysis, A.M.G.; resources, F.R.; data curation, A.M.G. and F.R.; writing—original draft preparation, A.M.G.; writing—review and editing, A.M.G. and F.R.; supervision, F.R.; funding acquisition, F.R. All authors have read and agreed to the published version of the manuscript.

**Funding:** This research received no external funding.

**Institutional Review Board Statement:** Not applicable.

**Informed Consent Statement:** Not applicable.

**Data Availability Statement:** Not applicable.

**Conflicts of Interest:** The authors declare no conflict of interest.

## References

1. Rossi, F.; Gambelli, A.M. Thermodynamic phase equilibrium of single-guest hydrate and formation data of hydrate in presence of chemical additives: A review. *Fluid Phase Equilibria* **2021**, *536*, 112958. [[CrossRef](#)]
2. Sloan, E.D.; Koh, C.A. *Clathrate Hydrates of Natural Gases*, 3rd ed.; Taylor & Francis Group: Boca Raton, FL, USA; CRC Press: New York, NY, USA, 2008.
3. Gambelli, A.M.; Rossi, F. Thermodynamic and kinetic characterization of methane hydrate nucleation, growth and dissociation processes, according to the Labile Cluster Theory. *Chem. Eng. J.* **2021**, *425*, 130706. [[CrossRef](#)]
4. Jeffrey, G.A. Hydrate inclusion compounds. *J. Incl. Phenom.* **1984**, *1*, 211–222. [[CrossRef](#)]
5. Pauling, L.; Marsh, R.E. The Structure of Chlorine Hydrate. *Proc. Natl. Acad. Sci. USA* **1952**, *38*, 112–118. [[CrossRef](#)] [[PubMed](#)]
6. Claussen, W.F. A Second Water Structure for Inert Gas Hydrates. *J. Chem. Phys.* **1951**, *19*, 1425–1426. [[CrossRef](#)]
7. Ripmeester, J.A.; Tse, J.S.; Ratcliffe, C.I.; Powell, B.M. A new clathrate hydrate structure. *Nature* **1987**, *325*, 135–136. [[CrossRef](#)]
8. Park, Y.; Kim, D.Y.; Lee, J.W.; Huh, D.G.; Park, K.P.; Lee, J.; Lee, H. Sequestering carbon dioxide into complex structures of naturally occurring gas hydrates. *Proc. Natl. Acad. Sci. USA* **2006**, *103*, 12690–12694. [[CrossRef](#)]
9. Lim, D.; Ro, H.; Seo, Y.; Seo, Y.J.; Lee, J.Y.; Kim, S.J.; Lee, J.; Lee, H. Thermodynamic stability and guest distribution of CH<sub>4</sub>/N<sub>2</sub>/CO<sub>2</sub> mixed hydrates for methane hydrate production using N<sub>2</sub>/CO<sub>2</sub> injection. *J. Chem. Thermodyn.* **2017**, *106*, 16–21. [[CrossRef](#)]
10. Durham, W.B.; Kirby, S.H.; Stern, L.A.; Zhang, W.U. The strength and rheology of methane clathrate hydrate. *J. Geophys. Res.* **2003**, *108*, 2182. [[CrossRef](#)]
11. Kashchiev, D.; Verdoes, D.; van Rosmalen, G.M. Induction time and metastability limit in new phase formation. *J. Cryst. Growth* **1991**, *110*, 373–380. [[CrossRef](#)]
12. Wang, S.R.; Yang, M.J.; Liu, W.G.; Zhao, J.F.; Song, Y.C. Investigation on the induction time of methane hydrate formation in porous media under quiescent conditions. *J. Pet. Sci. Eng.* **2016**, *145*, 565–572. [[CrossRef](#)]
13. Englezos, P.; Kalogerakis, N.; Dholabai, P.D.; Bishnoi, P.R. Kinetics of formation of methane and ethane gas hydrates. *Chem. Eng. Sci.* **1987**, *42*, 2647–2658. [[CrossRef](#)]
14. Sloan, E.D.; Fleyfel, F. A molecular mechanism for gas hydrate nucleation from ice. *AIChE J.* **1991**, *37*, 1281–1292. [[CrossRef](#)]
15. Rossi, F.; Li, Y.; Gambelli, A.M. Thermodynamic and kinetic description of the main effects related to the memory effect during carbon dioxide hydrates formation in a confined environment. *Sustainability* **2021**, *13*, 13797. [[CrossRef](#)]
16. Long, J. Gas Hydrate Formation Mechanism and Kinetic Inhibition. Ph.D. Thesis, Colorado School of Mines, Golden, CO, USA, 1994.
17. Radhakrishnan, R.; Trout, B.I. A new approach for studying nucleation phenomena using molecular simulations: Application to CO<sub>2</sub> hydrate clathrates. *J. Chem. Phys.* **2002**, *117*, 1786–1796. [[CrossRef](#)]
18. Jacobson, L.C.; Hujo, W.; Molinero, V. Amorphous Precursors in the Nucleation of Clathrate Hydrates. *J. Am. Chem. Soc.* **2010**, *132*, 11806–11811. [[CrossRef](#)]
19. Gambelli, A.M.; Presciutti, A.; Rossi, F. Kinetic considerations and formation rate of carbon dioxide hydrate, formed in presence of a natural silica-based porous medium: How initial thermodynamic conditions may modify the process kinetic. *Thermochim. Acta* **2021**, *705*, 179039. [[CrossRef](#)]
20. Gambelli, A.M.; Filipponi, M.; Rossi, F. How methane release may affect carbon dioxide storage during replacement processes in natural gas hydrate reservoirs. *J. Pet. Sci. Eng.* **2021**, *205*, 108895. [[CrossRef](#)]
21. Li, X.Y.; Feng, J.C.; Li, X.S.; Wang, Y.; Hu, H.Q. Experimental study of methane hydrate formation and decomposition in the porous medium with different thermal conductivities and grain sizes. *Appl. Energy* **2022**, *305*, 117852. [[CrossRef](#)]
22. Ripmeester, J.A.; Alavi, S. Some current challenges in clathrate hydrate science: Nucleation, decomposition and the memory effect. *Curr. Opin. Solid State Mater. Sci.* **2016**, *20*, 344–351. [[CrossRef](#)]
23. Li, Y.; Wu, N.; Ning, F.; Gao, D.; Hao, X.; Chen, Q.; Liu, C.; Sun, J. Hydrate-induced clogging of sand-control screen and its implication on hydrate production operation. *Energy* **2020**, *206*, 118030. [[CrossRef](#)]
24. Takeya, S.; Hori, A.; Hondoh, T.; Uchida, T. Freezing-Memory Effect of Water on Nucleation of CO<sub>2</sub> Hydrate Crystals. *J. Phys. Chem. B* **2000**, *104*, 4164–4168. [[CrossRef](#)]

25. Wu, Q.; Zhang, B. Memory Effect on the Pressure-Temperature Condition and Induction Time of Gas Hydrate Nucleation. *J. Nat. Gas Chem.* **2010**, *19*, 446–451. [[CrossRef](#)]
26. Duchateau, C.; Glénant, P.; Pou, T.E.; Hidalgo, M.; Dicharry, C. Hydrate Precursor Test Method for the Laboratory Evaluation of Kinetic Hydrate Inhibitors. *Energy Fuels* **2010**, *24*, 616–623. [[CrossRef](#)]
27. Bargherzadeh, S.A.; Mondrakovsky, I.L.; Ripmeester, J.A.; Englezos, P. Magnetic resonance imaging of gas hydrate formation in a bed of silica sand particles. *Energy Fuels* **2011**, *25*, 3083–3092. [[CrossRef](#)]
28. Kumar, A.; Sakpal, T.; Roy, S.; Kumar, R. Methane hydrate formation in a test sediment of sand and clay at various levels of water saturation. *Can. J. Chem.* **2015**, *93*, 874–881. [[CrossRef](#)]
29. Bhattacharjee, G.; Kumar, A.; Sakpal, T.; Kumar, R. Carbon dioxide sequestration: Influence of porous media on hydrate formation kinetics. *ACS Sustain. Chem. Eng.* **2015**, *3*, 1205–1214. [[CrossRef](#)]
30. Chong, Z.R.; Yaug, M.J.; Khoo, B.C.; Linga, P. Size effect of porous media on methane hydrate formation and dissociation in an excess gas environment. *Ind. Eng. Chem. Res.* **2016**, *55*, 7981–7991. [[CrossRef](#)]
31. Zang, X.Y.; Liang, D.Q.; Wu, N.Y. Gas hydrate formation in fine sand. *Sci. China Earth Sci.* **2013**, *56*, 549–556. [[CrossRef](#)]
32. Gambelli, A.M.; Rossi, F. Experimental investigation on the possibility of defining the feasibility of CO<sub>2</sub>/CH<sub>4</sub> exchange into a natural gas hydrate marine reservoir via fast analysis of sediment properties. *Chem. Eng. Res. Des.* **2021**, *171*, 327–339. [[CrossRef](#)]
33. Gambelli, A.M. Analyses on CH<sub>4</sub> and CO<sub>2</sub> hydrate formation to define the optimal pressure for CO<sub>2</sub> injection to maximize the replacement efficiency into natural gas hydrate in presence of a silica-based natural porous medium, via depressurization techniques. *Chem. Eng. Process.* **2021**, *167*, 108512. [[CrossRef](#)]
34. Hackikubo, A.; Takeya, S.; Chuvilin, E.; Istomin, V. Preservation phenomena of methane hydrate in pore spaces. *Phys. Chem. Chem. Phys.* **2011**, *13*, 17449–17452. [[CrossRef](#)] [[PubMed](#)]
35. Li, X.Y.; Li, X.S.; Wang, Y.; Li, G.; Zhang, Y.; Hu, H.Q.; Wang, K.; Zeng, H.P. Influence of particle size on the heat and mass transfer characteristics of methane hydrate formation and decomposition in porous media. *Energy Fuels* **2021**, *35*, 2153–2164. [[CrossRef](#)]
36. Gambelli, A.M.; Rossi, F. Formation rate as parameter to distinguish nucleation from hydrate massive growth phase: Experimental investigation in presence of two different porous media. *Exp. Therm. Fluid Sci.* **2022**, *131*, 110525. [[CrossRef](#)]
37. Sun, J.; Xin, Y.; Chou, I.M.; Sun, R.; Jiang, L. Hydrate Stability in the H<sub>2</sub>S–H<sub>2</sub>O system Visual Observations and Measurements in a High-Pressure Optical Cell and Thermodynamic Models. *J. Chem. Eng. Data* **2020**, *65*, 3884–3892. [[CrossRef](#)]
38. Wang, Y.; Feng, J.C.; Li, X.S.; Zhang, Y. Experimental investigation of optimization of well spacing for gas recovery from methane hydrate reservoir in sandy sediment by heat stimulation. *Appl. Energy* **2017**, *207*, 562–572. [[CrossRef](#)]
39. Yuan, Q.; Sun, C.Y.; Yang, X.; Ma, P.C.; Ma, Z.W.; Liu, B.; Ma, Q.L.; Yang, L.Y.; Chen, G.J. Recovery of methane from hydrate reservoir with gaseous carbon dioxide using a three-dimensional middle-size reactor. *Energy* **2012**, *40*, 47–58. [[CrossRef](#)]
40. Yin, Z.; Moridis, G.; Chong, Z.R.; Linga, P. Effectiveness of multi-stage cooling processes in improving the CH<sub>4</sub>-hydrate saturation uniformity in sandy laboratory samples. *Appl. Energy* **2019**, *250*, 729–747. [[CrossRef](#)]
41. Davidson, D.W.; Garg, S.K.; Gough, S.R.; Handa, Y.P.; Ratcliffe, C.I.; Ripmeester, J.A.; Tse, J.S.; Lawson, W.F. Laboratory analysis of a naturally occurring gas hydrate from sediment of the Gulf of Mexico. *Geochim. Cosmochim. Acta* **1986**, *50*, 619–623. [[CrossRef](#)]
42. Wang, X.; Dong, B.; Wang, F.; Li, W.; Song, Y. Pore-scale investigations on the effects of ice formation/melting on methane hydrate dissociation using depressurization. *Int. J. Heat Mass Transf.* **2019**, *131*, 737–749. [[CrossRef](#)]
43. Bavoh, C.B.; Partoon, B.; Lal, B.; Keong, L.K. Methane hydrate-liquid-vapor-equilibrium phase condition measurements in the presence of natural amino acids. *J. Nat. Gas Sci. Eng.* **2017**, *37*, 425–434. [[CrossRef](#)]
44. Bottger, A.; Kamps, A.P.S.; Maurer, G. An experimental investigation on the phase equilibrium of the binary system (methane + water) at low temperatures: Solubility of methane in water and three-phase (vapour + liquid + hydrate) equilibrium. *Fluid Phase Equilibria* **2016**, *407*, 209–216. [[CrossRef](#)]
45. Nagashima, H.D.; Ohmura, R. Phase equilibrium condition measurements in methane clathrate hydrate forming system from 197.3 K to 238.7 K. *J. Chem. Thermodyn.* **2016**, *102*, 252–256. [[CrossRef](#)]
46. Kassim, Z.; Khan, M.S.; Lal, B. Thermodynamic modelling on methane hydrate equilibrium condition in the presence of electrolyte inhibitor. *Mater. Today* **2019**, *19*, 1395–1402. [[CrossRef](#)]
47. Khan, M.S.; Partoon, B.; Bavoh, C.B.; Lal, B.; Mellon, B.M. Influence of tetramethylammonium hydroxide on methane and carbon dioxide gas hydrate phase equilibrium conditions. *Fluid Phase Equilibria* **2017**, *440*, 1–8. [[CrossRef](#)]
48. Seo, Y.T.; Lee, H. Multiple-phase hydrate equilibria of the ternary carbon dioxide, methane, and water mixtures. *J. Phys. Chem. B* **2001**, *105*, 10084–10090. [[CrossRef](#)]
49. Sangway, J.S.; Oellrich, L. Phase equilibrium of semiclathrate hydrates of methane in aqueous solutions of tetra-n-butyl ammonium bromide (TBAB) and TBAB-NaCl. *Fluid Phase Equilibria* **2014**, *367*, 95–102. [[CrossRef](#)]
50. Semenov, A.P.; Medvedev, V.I.; Guschin, P.A.; Yakushev, V. Effect of heating rate on the accuracy of measuring equilibrium conditions for methane and argon hydrates. *Chem. Eng. Sci.* **2015**, *137*, 161–169. [[CrossRef](#)]
51. Shu, S.; Tiwikrama, A.H.; Yang, C.; Lee, M. Phase equilibrium and dynamic behavior of methane hydrates decomposition via depressurization in the presence of a promoter tert-butanol. *J. Taiwan Inst. Chem. Eng.* **2019**, *95*, 119–130. [[CrossRef](#)]